Received 3 February 2022
Revised 1 March 2022
Accepted 22 April 2022

The coupled vibration of train and bridge as high-speed trains meet in crosswind

Wenhua Guo
School of Civil Engineering, Central South University, Changsha, China
Xinmin Hong
School of Civil Engineering, Hunan City University, Yiyang, China, and
Chunxia Chen
Highway Design and Research Institute, Zhejiang Provincial Institute of Communications Planning Design and Research, Hangzhou, China

Abstract

Purpose – This paper aims to study the influence of aerodynamics force of trains passing each other on the dynamic response of vehicle bridge coupling system based on numerical simulation and multi-body dynamics and put forward the speed threshold for safe running of train under different crosswind speeds.

Design/methodology/approach – The computational fluid dynamics method is adopted to simulate the aerodynamic force in the whole process of train passing each other by using dynamic grid technology. The dynamic model of vehicle-bridge coupling system is established considering the effects of aerodynamic force of train passing each other under crosswind, the dynamic response of train intersection on the bridge under crosswind is computed and the running safety of the train is evaluated.

Findings – The aerodynamic force of trains' intersection has little effects on the derailment factor, lateral wheel-rail force and vertical acceleration of train, but it increases the offload factor of train and significantly increases the lateral acceleration of train. The crosswind has a significant effect on increasing the derailment factor, lateral wheel-rail force and offload factor of train. The offload factor of train is the key factor to control the threshold of train speed. The impact of the aerodynamic force of trains' intersection on running safety cannot be ignored. When the extreme values of crosswind wind speed are 15 $m \cdot s^{-1}$, 20 $m \cdot s^{-1}$ and 25 $m \cdot s^{-1}$, respectively, the corresponding speed thresholds for safe running of train are 350 $km \cdot h^{-1}$, 275 $km \cdot h^{-1}$ and 200 $km \cdot h^{-1}$, respectively.

Originality/value – The research can provide a more precise numerical method to study the running safety of high-speed trains under the aerodynamic effect of trains passing each other on bridge in crosswind.

Keywords High-speed railway, Trains passing each other, Vehicle-bridge coupling system, Crosswind, Speed threshold

Paper type Research paper

1. Introduction

With bridge extensively adopted in China's high-speed railway as the substitute for the subgrade, the new approach ensures the safety, stability and riding comfort of high-speed

This research was supported by the National Natural Science Foundation of China (Project no. 52078489) and the Fundamental Research Funds for the Central Universities of Central South University (Project no. 2021zzts0772) to which the authors are most grateful.

Railway Sciences
Vol. 1 No. 2, 2022
pp. 260-272
Emerald Publishing Limited
e-ISSN: 2755-0915
p-ISSN: 2755-0907
DOI 10.1108/RS-04-2022-0021

trains and minimizes the use of agricultural lands. With high-bridge ratio (in some lines even exceeding 90% (He *et al.*, 2017)) as a distinctive feature, it is very likely to encounter the meeting of trains on a bridge. Due to the viscosity of air, the aerodynamic force of high-speed trains changes sharply as they meet (Huang, Li, & Yang, 2019; Lu, Zhang, Zheng, Lu, & Wu, 2018), and the rapid change increases train vibration. The train may derail or even rollover due to strong crosswind during running (Miao, Tian, & Gao, 2010; Hu & Guo, 2009). Under the combined action of strong crosswind and the aerodynamic force of train intersection, the riding comfort of passengers will be greatly compromised, and the possibility of derailment and overturning of trains will increase.

Scholars at home and abroad have conducted numerical simulations, wind tunnel tests, real train tests, etc. to study the aerodynamic force amid trains intersection and the operation safety of high-speed trains under crosswind. Li, Yang, Wu and Qiang (2015) studied the aerodynamic characteristics of trains passing each other on the bridge under crosswind through numerical simulation. Qiu, Li, Sha, Xiao and Wang (2018) carried out simulation when a train passes through a stopped train on single track in a wind tunnel test and analyzed the influence of train speed, wind speed, synthetic wind angle and other parameters on the aerodynamic coefficient amid train intersection. Zhai, Li, Zhang and Lv (2013) analyzed the influence of bridge height on the running safety of trains passing each other with the help of dynamic grid technology and numerical simulation. Chen, Zhang, He and Huang (2014) conducted onsite test to study the aerodynamic action of high-speed trains passing each other in tunnels. Tian, Xu, Liang and Liu (2006) and Xiong and Liang (2009) measured the air pressure wave as CRH_2 trains meet at a constant speed of 250 $km \cdot h^{-1}$ and obtained the conclusion that the track distance of 4.4 m will not affect the train's running safety. Guo and Zeng (2001) and Zhang, Xia, Guo and Xia (2009) analyzed the vehicle-bridge coupling dynamic response as a train passes through a large-span cable-stayed bridge of single track under the action of fluctuating wind, evaluated the train operation safety and proposed the speed limits of trains under different wind speeds.

In the above studies, only the influence of the train intersection on train aerodynamic force or the influence of crosswind on single-track train running safety was considered, while the influence of aerodynamic force of train intersection on train operation safety has been largely overlooked. In the current wind tunnel test, it is not possible to simulate train intersection for the study of the aerodynamic force in the process, which is generally calculated according to the aerodynamic coefficient of the relative positions of trains with the influence of train movement on the surrounding flow field ignored.

In this paper, the aerodynamic force of the meeting of two trains with three-car formation is simulated and calculated with the help of dynamic grid technology and numerical simulation. The time course is extended to that of eight-car formation trains with the help of a self-compiled program. The aerodynamic forces of the train and the bridge are applied to the 3D dynamic analysis model of wind-train-multi-span simply-supported beam jointly established by SIMPACK software and ANSYS software, and the dynamic response of train intersection on the multi-span simply-supported beam bridge under crosswind is studied. According to the safety index of train running, the speed threshold for safe running with consideration to the aerodynamic force of train intersection under crosswind is put forward.

2. Aerodynamic forces of train and bridge

2.1 Six components of aerodynamic force on train

In the natural wind field, the aerodynamic force acting on the high speed train is shown in Figure 1, including lateral force F_x, resistance F_y, lift force F_z, pitching moment M_x, roll moment M_y and lateral deflection moment M_z.

2.2 Three components of aerodynamic force on bridge

When natural wind flows through the bridge, the bridge is subject to the aerodynamic force formed by aerodynamic (Han & Cai, 2009), including aerodynamic drag force F_D, lift force F_L and moment F_M, as shown in Figure 2.

2.3 Calculation model of aerodynamic force of train intersection

Using FLUENT software as the calculation platform, the paper adopts dynamic grid technology to establish a 1:1 full-scale 3D model for the intersection of two trains on a bridge and calculate the aerodynamic force of the trains under crosswind during the intersection on bridge. The flow field as the trains meet on the bridge is considered a viscous, incompressible and inconstant one, and the turbulent movement caused by the high-speed movement of the train is studied by the reynolds average navier-stokes method. Given the calculation capacity of the computer and the similar aerodynamic characteristics of the intermediate cars, the train of three car formation (head car, intermediate car and tail car, 25.25 m long, 3.27 m wide and 3.82 m high each) is used for numerical simulation. The bridge in simulation is a 32 m-long double-track simply-supported beam, which is commonly used in the China high-speed railway, with a total of seven spans. On the premise of calculation accuracy and speed, the influence of train windows, pantographs, bridge guardrails and tracks are waived. The calculation area and the overall coordinate system are shown in Figure 3 (Hong, 2020), which registers 300, 240 and 60 m in length, width and height. The flow field is divided with the help of unstructured tetrahedral meshes which are radioactive. The meshes near the train and the bridge are comparatively small, and the meshes far away from these components are appropriately enlarged so as to ensure the calculation accuracy within the calculation workload. The minimum mesh size of the whole area is 0.2 m, and the total number of meshes is about 3,994,500. Train movement is achieved by editing the user define function program. Train movement causes mesh deformation. When the mesh quality is lower than a certain value, the local low-quality meshes are updated by the local remeshing method and smoothing method to ensure the mesh quality and the results accuracy amid train movement. At the beginning, the distance between the nose tips of the head cars of the two trains is 72 m, which is recorded as 72 m. During the analysis, the trains are considered to pass each other at a constant speed, and the crosswind direction is perpendicular to the train operation direction.

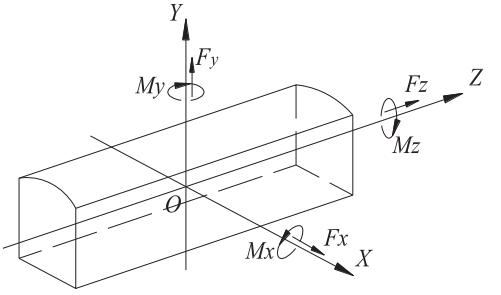

Figure 1.
Schematic diagram of six components of aerodynamic force on train

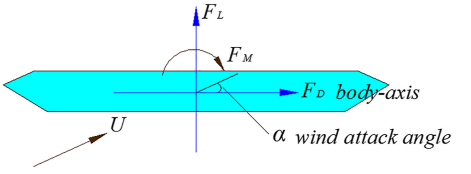

Figure 2.
Schematic diagram of three components of aerodynamic force on bridge

2.4 Aerodynamic force results of train intersection

According to the above-mentioned aerodynamic force calculation model for train intersection, the paper calculates the time course of the aerodynamic force amid trains' intersection at the speed of 350 km/h without crosswind. In order to facilitate the analysis, the analyzed train is named train A, and the train in the opposite direction is named train B. The aerodynamic force results of the head car and the intermediate car are shown in Figure 4. From Figure 4, the following laws can be found.

(1) Due to the viscosity of the air, the head car and intermediate car of the train are subjected to outward lateral force when the head car and the intermediate car of train A meet with the head car and the intermediate car of train B, respectively, while the head car and intermediate car of the train are subjected to inward lateral force when the head car and the intermediate car of train A leave each other with the head car and the intermediate car of train B, respectively. The lateral forces of the head cars are greater than that of the intermediate car.

(2) Before the two trains meet, the head cars are subjected to downward lift, and the lift of the intermediate cars are basically zero; the head cars and intermediate cars receive additional upward force when two trains meet; the head cars and intermediate cars are subjected to additional downward force when the trains leave each other; the variation amplitude of the lift of the head cars are about twice that of the intermediate cars.

(3) In the whole process of intersection, the head cars of the train are subjected to drag force opposite to the forward direction of trains. The drag forces of the head cars increase first, then decrease and finally increase to the size before intersection. Due to the shielding effect of the head car, the drag forces of the intermediate cars are almost equal to zero, which is far less than that of the head car.

(4) Because the two trains are moving in the opposite direction, the pitch moments of the two trains are equal and in the directions are opposite. Due to the shielding effect of the head car, the pitch moments of the intermediate car are much smaller than that of the head car. There is a sudden change in the pitch moments of the trains when the train meets and leaves each other.

(5) Due to the two trains have the opposite direction of advance, the values of the yaw moments of the two trains are equal and the direction is the same. The variation range of the yaw moments of the head cars and the intermediate cars are basically the same.

(6) The roll moment of the head cars and the intermediate cars are basically zero before and after the trains intersection, and there are two sudden changes in the whole

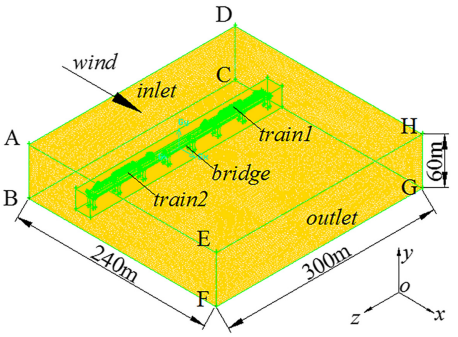

Figure 3.
Calculation area and overall mesh distribution (unit: m)

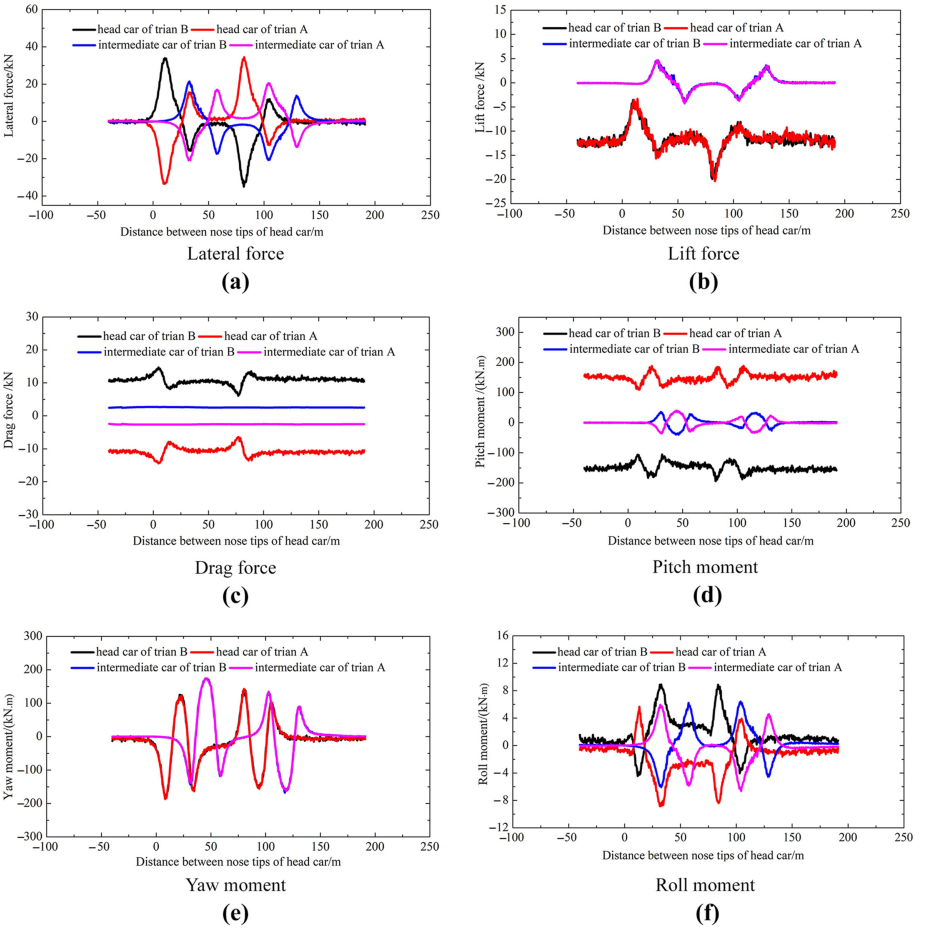

Figure 4.
Time course curve of aerodynamic force of the head car and the intermediate car of two intersected trains of three-car formation

process of trains intersection. The change trend of the roll moment of trains just echoes with the change trend of lateral force of trains, and the roll moment of the intermediate cars are less than that of the head cars.

(7) Due to the sequence of trains intersection, the start time and the end time of aerodynamic change of intermediate cars are a little later than that of the head car.

Given the similarity in the aerodynamic force of the intermediate cars, the paper in accordance with the needs of study extends the time course curve of the intersection of trains of three-car formation to one for the meeting of eight-car formation trains. Figure 5 shows the time course curve of the lateral force of the head car during the intersection of two trains of eight-car formation.

3. Mechanical model of wind–train–bridge coupling system

3.1 Vehicle dynamics model

The vehicle model is of secondary suspension and four axles, which consists of seven rigid bodies, including one carbody, two bogies and four wheelsets. Each rigid body has six

degrees of flexibility, including expansion, sway, bouncing, rolling, pitching and yawing. A single car has 42 degrees of freedom in total, as shown in Figure 6. In the figure: x_c, y_c, z_c, θ_c, φ_c and ψ_c are the degrees of freedom of the carbody in *x*, *y*, *z*, θ, φ and ψ directions, respectively; x_t, y_t, z_t, θ_t, φ_t and ψ_t are the degrees of freedom of bogie in *x*, *y*, *z*, θ, φ and ψ directions, respectively; x_w, y_w, z_w, θ_w, φ_w and ψ_w are the degrees of freedom of wheelsets in *x*, *y*, *z*, θ, φ

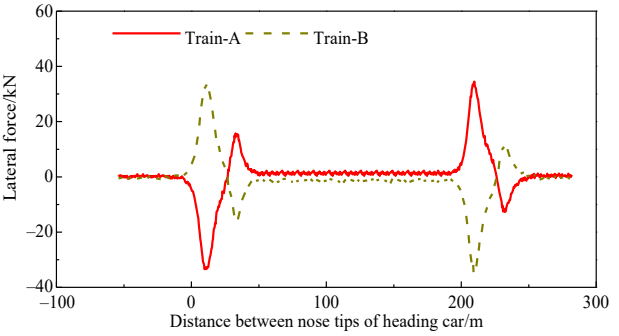

Figure 5.
Time course curve of lateral force of head cars of two trains with eight-car formation passing each other

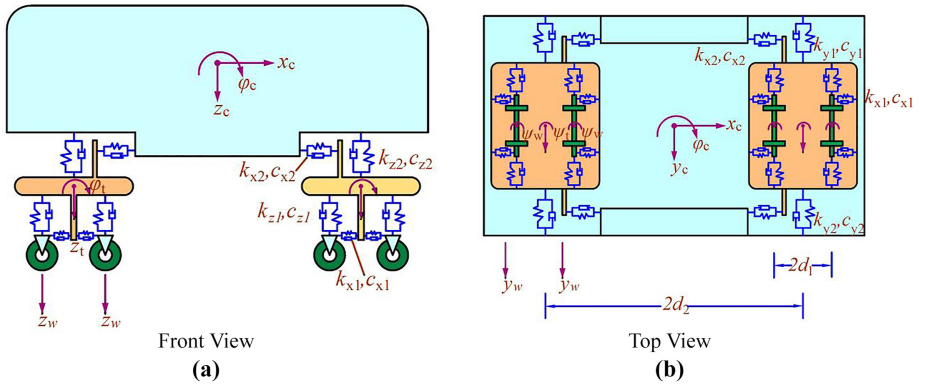

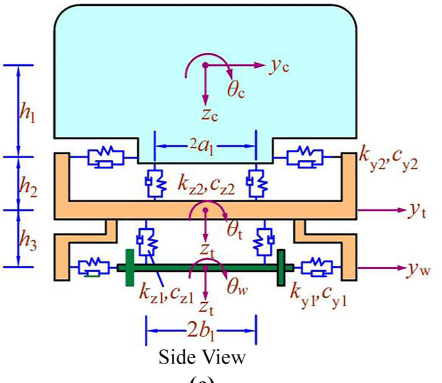

Figure 6.
Schematic diagram of vehicle dynamics model

and ψ directions, respectively. $2d_1$ and $2d_2$ are the wheelset spacing and bogie spacing, respectively; $2a_1$ and $2b_1$ are the transverse distances of secondary suspension and primary suspension, respectively; h_1,h_2 and h_3 are the heights of car centroid, secondary suspension vertex and secondary suspension vertex to bogie centroid and bogie centroid to wheelset centroid, respectively; c_{x1}, c_{y1}, c_{z1}, k_{x1}, k_{y1} and k_{z1} are the damping and stiffness of primary suspension in x, y and z directions, respectively; c_{x2}, c_{y2}, c_{z2}, k_{x2}, k_{y2} and k_{z2} are the damping and stiffness of secondary suspension in x, y and z directions, respectively (Guo, Hong, & Wang, 2020).

3.2 Dynamic models of bridge and track structure

The bridges, tracks and piers are simulated by spatial beam elements in the finite element analysis. The track, considered the Euler beam supported by discrete elastic points, is connected with the main girder by fasteners, therefore seen as spring-damping elements. The stiffness of the pier foundation is superimposed on the corresponding nodes. The damping of the bridge system is considered as Rayleigh damping, and the damping ratio at low frequency is 2–5% generally. Secondary dead load of the bridge is considered part of the mass of the main girder.

3.3 Implementation of wind–train–bridge coupling simulation

The coupling vibration of train–bridge system involves two sub-systems of train and bridge. The finite element model of bridge is established on ANSYS and imported into SIMPACK to form the a vehicle/train–bridge coupling vibration dynamic analysis model with the vehicle model and track model. The track irregularity is used as the internal excitation of coupling system, while the aerodynamic forces of train and bridge are used as the external excitation of vehicle/train–bridge coupling system and are applied to the coupling system via No. 93 force element in SIMPACK. On the wheel–rail contact surface, discrete information points are used for the exchange of data on displacement, speed and force to realize the simulation analysis of coupling vibration (Zhu, Qi, & Jia, 2014). In the vibration calculation, the train is regarded as a rigid body and the bridge as a flexible one. Different algorithms are used to solve their kinematic equations, backward differential formula for the train and modal superposition method for the bridge. The two are solved in turn and in iteration within time step, as shown in Figure 7. The wheel–rail normal force is calculated using the Hertz nonlinear contact theory, and the wheel–rail tangential creep force is calculated using the simplified Kalker creep assumption (Du, Xu, & Xia, 2012).

4. Calculation examples

4.1 Basic parameters of models

The 32 m-long seven-span double-track simply-supported bridge, commonly used in high-speed railway, is taken as the object of study with the track distance being 5.0 m. The main girder is of box-shaped section and C50 concrete. The net width of the bridge deck is 13.4 m, the beam height is 3.05 m, the beam length is 32.6 m and the net span is 31.5 m. Secondary dead load of 184 $\mathrm{kN \cdot m^{-1}}$ is considered to be equivalent to the mass of the main girder. The pier adopts C30 concrete pier of hollow rectangular section, with a longitudinal length of 3.3 m, a transverse length of 6.8 m, a wall thickness of 0.5 m and a pier height of 16 m. The pier bottom support is considered to be consolidated. The elastic modulus E and Poisson's ratio μ of the material are determined according to the current bridge regulations, and the model damping ratio is 0.02. The train adopts German ICE3 high speed train. Refer to reference (Chen, 2019) for vehicle parameters. The train formation is as follows: 1 motor car + 6 trailer cars + 1 motor car. The track structure adopts bi-block ballastless track. The rail adopts

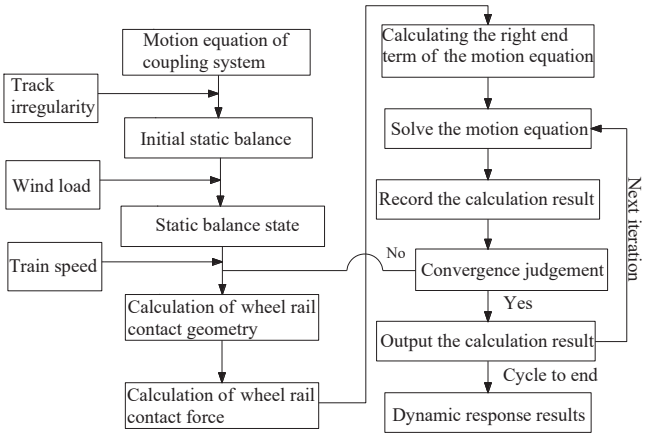

Figure 7.
Iteration diagram of train–bridge system's solution

standard 60 rail, with a track length and gauge being 660 m and 1.5 m. The set spacing of fasteners is 0.6 m, the lateral stiffness of fasteners is 60 $MN \cdot m^{-1}$, the vertical stiffness is 120 $MN \cdot m^{-1}$, the lateral damping is 0.12 $MN \cdot s \cdot m^{-1}$, and the vertical damping is 0.15 $MN \cdot s \cdot m^{-1}$. According to the suggestions in the *Technical Conditions for High Speed Test Trains* in China, the simulation of track irregularity is conducted with the help of the German track low interference spectrum, in which the spatial step length is 0.2 m.

4.2 Influence of aerodynamic force of train intersection without crosswind on the dynamic response of train

The paper aims to unveil the aerodynamic force amid train intersection with no crosswind and its impact on the dynamic response of the vehicle/train–bridge coupling system. In this sense, it calculates the vibration response of train both intersecting and not intersecting another train at 350 $km \cdot h^{-1}$ in a no crosswind environment. The dynamic response of the head car of the train is shown in Figure 8.

It can be seen from Figure 8 that the dynamic response of the train in the non-crosswind environment is mainly caused by track irregularity, and the vibration response is closely related to track irregularity; in both cases with and without the aerodynamic force of train intersection, the time course of the derailment coefficient, the lateral wheel–rail force as well as the time course of vertical acceleration generally follows the same trends. With consideration of the aerodynamic force of train intersection, the wheel load reduction rate of the train increases; the aerodynamic force of train intersection significantly increases the lateral acceleration of the train, which increases significantly near 3.5 s and 4.5 s, and it is caused by the sudden change of the aerodynamic force on the train at the beginning and the ending of intersection.

4.3 Influence of aerodynamic force of train intersection under crosswind on dynamic response of train

In order to study the impact of the aerodynamic force of train intersection under crosswind on the vibration response of the vehicle–bridge coupling system, the paper calculates the vibration response of trains passing on the bridge at 350 $km \cdot h^{-1}$ both with and without aerodynamic force of train intersection under the crosswind speed at 10 $m \cdot s^{-1}$. Please refer to Figure 9 for the dynamic response of the head car.

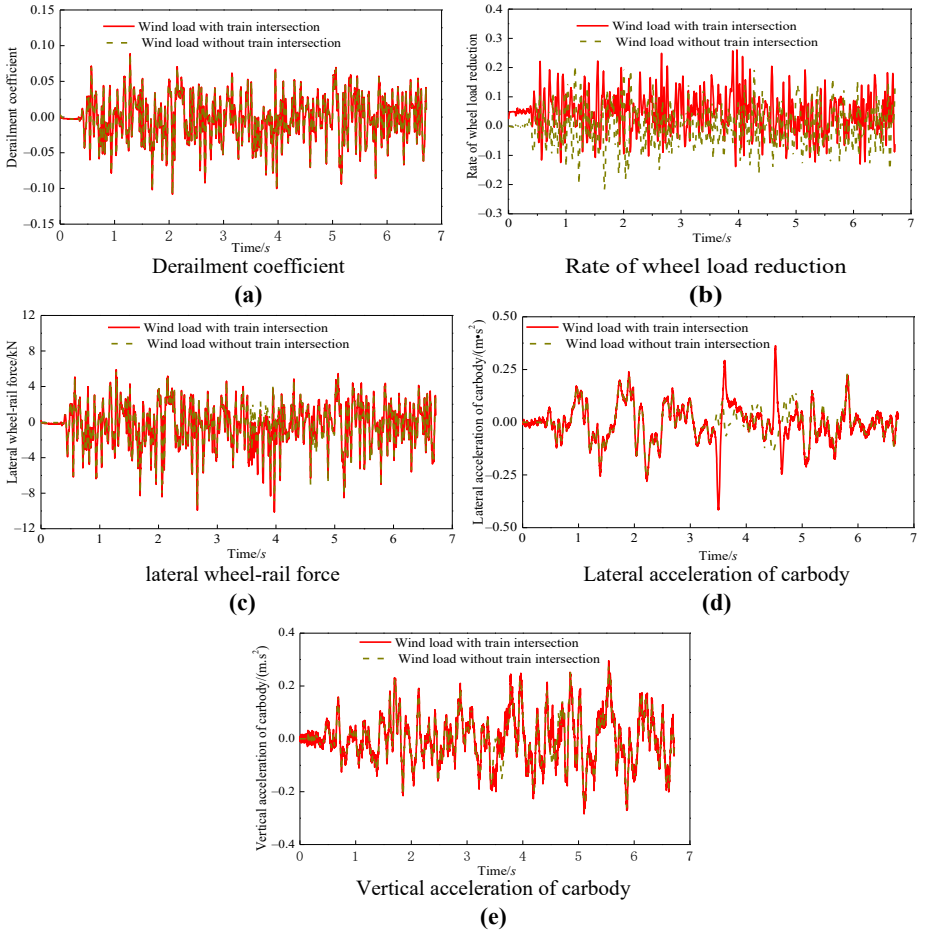

Figure 8.
Time course of dynamic response of head car with no crosswind

The comparison of Figures 8 and 9 shows that the crosswind significantly increases the derailment coefficient, the wheel load reduction rate and the lateral wheel-rail force of trains, and the effects of crosswind on the lateral and vertical accelerations of trains are relatively small; the aerodynamic force of train intersection under crosswind has a significant effect on the rise of the lateral acceleration of the train, and at the same time, it pushes up the wheel load reduction rate by a large margin.

4.4 Speed threshold for trains intersection in crosswind

In order to ensure the running safety in crosswind, the high speed railway authorities set corresponding threshold of running speed under different levels of crosswind. The dynamic response of trains' intersection at different speeds under crosswind is calculated. The crosswind speed increases with a gradient of 5 $m \cdot s^{-1}$ in the range of 0–25 $m \cdot s^{-1}$, and the vehicle speed changes with a gradient of 25 $km \cdot h^{-1}$ in the range of 200–350 $km \cdot h^{-1}$. A total of 42 working conditions are calculated. The train dynamic response amid the intersection of trains running at 300 $km \cdot h^{-1}$ under 20 $m \cdot s^{-1}$ crosswind is shown in Figure 10. It can be seen

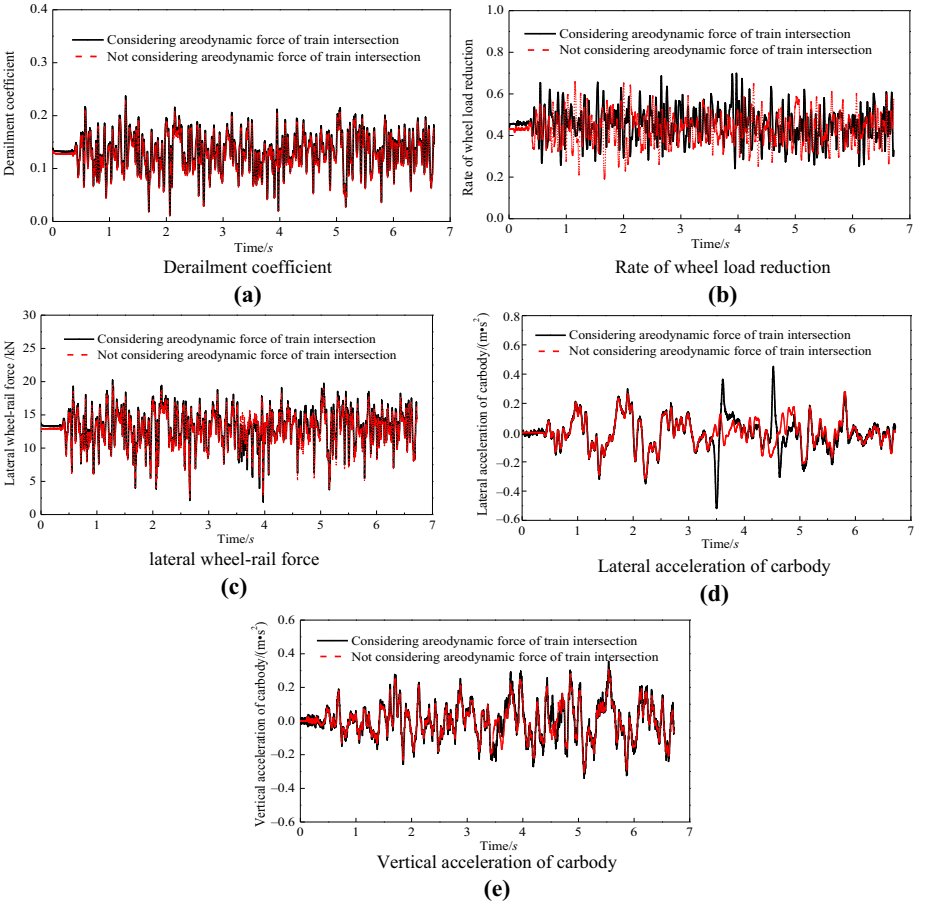

Figure 9.
Head car dynamic response time course

that the derailment coefficient, lateral wheel-rail force and wheel load reduction rate of the trains tend to increase amid intersection, while the derailment coefficient, lateral wheel–rail force as well as the wheel load reduction rate of the head car largely exceed those of the intermediate and the tail cars. Figure 10a show that during the whole process of train intersection, the wheel load reduction rate of the head car exceeds the specification limit at the time when the two head cars meet and the two tail cars leave each other, while the wheel load reduction rate of the intermediate car and the tail car are less than the specification limit.

Figure 11 shows the dynamic response of the trains passing each other at a speed of 200–350 $km \cdot h^{-1}$ at a crosswind speed of 0–25 $m \cdot s^{-1}$. The dotted horizontal line in the figure is the safety limits of the dynamic response of trains specified in the relevant technical specification. It can be seen from Figure 10 that the derailment coefficient, lateral wheel-rail force and wheel load reduction rate of the train increase with the rise of wind speed and train speed; under each working condition, the derailment coefficient and lateral wheel–rail force of the train meet the requirements of relevant specifications. However, in some cases, the wheel load reduction rate of the train exceeds the specified limits, which makes the rate the control index for the safe intersection of trains on the bridge.

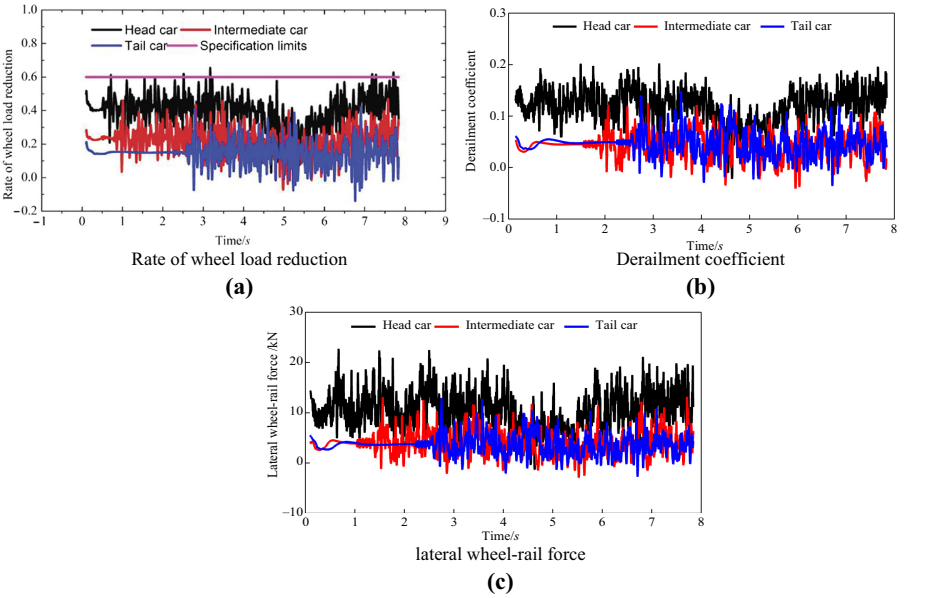

Figure 10.
Time course of dynamic response of trains' intersection at speed of 300 km·h^{-1} under 20 m·s^{-1} crosswind

It can also be seen from Figure 11b that when the crosswind speed is less than 15 m·s^{-1} and the trains pass each other at a speed of 350 km·h^{-1}, the maximum wheel load reduction rate of the train is 0.548, which is less than the safety limit of 0.6 specified in relevant specifications. Therefore, when the crosswind speed is less than 15 m·s^{-1}, the speed threshold shall be 350 km·h^{-1}. When the crosswind speed is between [15, 20] m·s^{-1} and the trains pass each other at 300 km·h^{-1}, the maximum wheel load reduction rate is 0.618; when the trains pass each other at 275 km·h^{-1}, the maximum wheel load reduction rate is 0.578; when the crosswind speed is [15, 20] m·s^{-1}, the speed threshold is 275 km·h^{-1}; when the crosswind speed is between [20, 25] m·s^{-1} and the trains pass each other at 225 km·h^{-1}, the maximum wheel load reduction rate of the train is 0.631; when the trains pass each other at 200 km·h^{-1}, the maximum wheel load reduction rate of the train is 0.589; when the crosswind speed is [20, 25] m·s^{-1}, the train speed threshold shall be 200 km·h^{-1}.

5. Conclusion

(1) Given the similarity of the aerodynamics characteristics of intermediate cars, the time course of the aerodynamic force of the intersection of trains of three-car formation can be extended to one of eight-car formation passing.

(2) The crosswind plays a significant role in the increase of the wheel load reduction rate, the lateral wheel–rail force as well as the derailment coefficient and has no obvious impact on the train acceleration.

(3) The aerodynamic force of train intersection has a significant impact on the lateral acceleration of the train and has, to some extent, push up the wheel load reduction ratio of the train but has no obvious effect on other dynamic responses of the train.

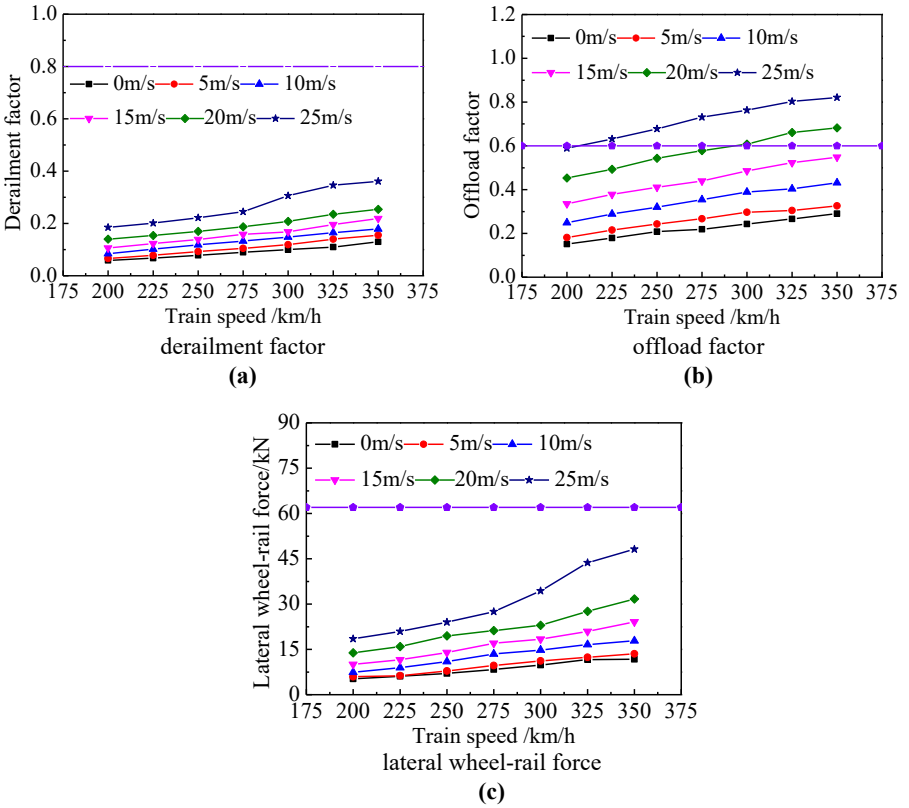

Figure 11.
Relation between train dynamic response and speed at different wind speeds

(4) The train wheel load reduction rate is the key index to control the speed threshold. The impact of the aerodynamic force amid train intersection on the running safety of trains shall not be overlooked.

References

Chen, C. X. (2019). *Vibration response Analysis of Train-rail-bridge Coupling System for High-speed Train Intersection Under Crosswind*. Master dissertation. Changsha: Central South University. in Chinese.

Chen, H. C., Zhang, Y., He, D. H., & Huang, C. R. (2014). Experimental study on the basic laws of the aerodynamic effect of 350 km·h^{-1} high speed railway tunnel. *China Railway Science*, *35*(1), 55–59, in Chinese.

Du, X. T., Xu, Y. L., & Xia, H. (2012). Dynamic interaction of bridge-train system under non-uniform seismic ground motion. *Earthquake Engineering and Structural Dynamics*, *41*(1), 139–157.

Guo, X. R., & Zeng, Q. Y. (2001). Analysis of critical wind speed for running trains on a schemed Yangtze River bridge at Nanjing on Jing-Hu high speed railway line. *Journal of the China Railway Society*, *23*(5), 75–80, in Chinese.

Guo, W. H., Hong, X. M., & Wang, Z. H. (2020). Seismic isolation analysis of friction pendulum bearing on coupling system of high-speed train and simply supported beam bridge. *Journal of Southeast University: Natural Science*, *50*(2), 267–273, in Chinese.

Han, Y., & Cai, C. S. (2009). The aerodynamic characteristics of the vehicle and bridge for the coupled wind-vehicle-bridge system. *Journal of Changsha University of Science and Technology: Natural Science*, *6*(4), 21–27, in Chinese.

He, X. H., Wu, T., Zou, Y. F., Chen, Y. F., Guo, H., & Yu, Z. W. (2017). Recent development of high-speed railway bridges in China. *Structure and Infrastructure Engineering*, *13*(12), 1584–1595.

Hong, X. M. (2020). *Study on the Coupled Vibration of High-speed Train and long Span Cable-stayed Bridge System Under the Aerodynamic Effect of Trains Passing Each other in Crosswind*. Doctoral dissertation. Changsha: Central South University. in Chinese.

Hu, S. L., & Guo, W. H. (2009). Aerodynamic characteristics of high speed vehicle and bridge in the crosswind. *Journal of Chongqing Jiaotong University: Natural Science*, *28*(6), 1008–1010, in Chinese.

Huang, S., Li, Z. W., & Yang, M. Z. (2019). Aerodynamics of high-speed maglev trains passing each other in open air. *Journal of Wind Engineering and Industrial Aerodynamics*, *188*(5), 151–160.

Li, Y. L., Yang, Y., Wu, M. X., & Qiang, S. Z. . (2015). Aerodynamic characteristics in the process of two trains passing each other on bridge under cross wind action. *China Railway Science*, *36*(2), 37–44, In Chinese.

Lu, Y. H., Zhang, D. W., Zheng, H., Lu, C., & Wu, P. (2018). Analysis of the aerodynamic pressure effect on the fatigue strength of the carbody of high-speed trains passing by each other in a tunnel. *Proceedings of the Institution of Mechanical Engineers*, *233*(8), 783–801.

Miao, X. J., Tian, H. Q., & Gao, G. J. (2010). The influence of the gorge wind on the aerodynamic performance of the train on bridge. *China Railway Science*, *31*(6), 63–67, In Chinese.

Qiu, X. W., Li, X. Z., Sha, H. Q., Xiao, J., & Wang, M. (2018). Wind tunnel measurement of aerodynamic characteristics of trains passing each other on truss bridge. *China Journal of Highway and Transport*, *31*(7), 76–83, in Chinese.

Tian, H. Q., Xu, P., Liang, X. F., & Liu, T. H. (2006). Correlation between pressure wave of train passing and running speed. *China Railway Science*, *27*(6), 64–67, in Chinese.

Xiong, X. H., & Liang, X. F. (2009). Analysis of air pressure pulses in meeting of CRH_2 EMU trains. *Journal of the China Railway Society*, *31*(6), 15–20, in Chinese.

Zhai, J. P., Li, M., Zhang, J. Y., & Lv, F. M. (2013). Influence of bridge height on passing performance of high speed trains under crosswind. *Computer Aided Engineering*, *22*(3), 1–8, in Chinese.

Zhang, N., Xia, H., Guo, W. W., & Xia, C. Y. (2009). Analysis on the wind-vehicle-bridge coupling vibration for Nanjing Dashengguan Yangtze River bridge of Beijing-Shanghai high-speed railway. *China Railway Science*, *30*(1), 41–48, in Chinese.

Zhu, W., Qi, T., & Jia, L. (2014). Dynamic performance analysis of vehicle-bridge system for a cable-stayed bridge with steel truss girder based on SIMPACK. *Railway Standard Design*, *58*(7), 89–94, in Chinese.

Corresponding author
Wenhua Guo can be contacted at: whguo@csu.edu.cn